# RF Capacitive Spectroscopy for Contactless Measurements of Resistivity Profiles in Highly Resistive Semiconductor Wafers

Jerzy Krupka and Jaroslaw Judek

*Abstract*—**In this paper, we present a contactless, capacitive method of estimating the resistivity profiles in the direction perpendicular to the semiconductor wafer using frequency domain impedance analysis. Employing a simple model, we show that the different resistivity distributions inside a wafer affect the frequency dependencies of the measured effective capacitance and the Q-factor. We also demonstrate how to estimate resistivity variation inside the sample from the experimental data: C(ω) and Q(ω).**

*Index Terms*—**Measurements, capacitance measurements, Gallium compounds.**

## I. Introduction

RESISTIVITY is one of the most important parameter for quality control of virgin wafers, in semiconductor industry. For many applications high resistivity semiconductors are employed. Among them are such materials as silicon (Si), gallium phosphide (GaP) gallium arsenide (GaAs), gallium nitride (GaN) and silicon carbide (SiC). To obtain high resistivity (semi-insulating) semiconductor the highest purity starting materials must be used during the crystal growth. It should be pointed out that to obtain semi-insulating silicon having resistivity $> 10^4$ Ωcm, the amount of uncompensated impurities such as boron or phosphorous should be $< 10^{12}$ cm$^{-3}$. In practice it is almost impossible to get such low impurity level. For this reason one common way to obtain high resistivity semiconductors is to compensate acceptor impurities by appropriate amount of donors or vice versa. This can be done employing different methods e.g., by adding dopants in the growth chamber during the pulling of the crystals or by neutron doping technique. The problem is that initial residual impurities are usually not uniformly distributed in the crystal so it is very difficult to compensate them at every point of the crystal. As the result semi-insulating semiconductors always exhibit resistivity variations. Manufacturers of high resistivity semiconductor wafers specify parameter that is called radial resistivity variation. For silicon wafers having diameter of 100-150 mm and resistivity $> 10^4$ Ωcm the radial resistivity variation is typically $< 25\%$. Wafers made of semiconductor compounds such as SiC or GaN in the addition to radial resistivity variation may exhibit also resistivity variation in the direction perpendicular to the wafer. Such variations have two origins, the first is non-uniform distribution of dopants and the second is the influence of the surface states (in-built surface charges and Fermi level bending on the semiconductor surfaces) on the distribution of free charge carriers near surfaces of the wafer.

Capacitive time domain [1] and frequency domain [2]–[4] methods are commonly used for contactless measurement of conductivity and the sheet resistance of highly resistive semiconductors and constitute a branch of impedance spectroscopy [5]. In fact the capacitive methods are the only ones, among the contact-less techniques, that allow resistivity measurements in the range above $10^6$ Ωcm. The standard resistivity measurement range for commercially available capacitive time-domain mapping instruments is from $10^6$ Ωcm to $10^9$ Ωcm and the extended measurement range is from $10^5$ Ωcm to $10^{12}$ Ωcm. Resistivity distribution in the direction perpendicular to the sample is not evaluated in the commercially available AC impedance methods, although the presence of depletion layers has been observed in frequency domain experiments, especially for silicon samples see [3].

The main objective of this paper is to describe in details capacitive frequency domain method, which was initially proposed at the conference [7], which not only allows determination of the bulk resistivity of the sample but also determination of resistivity and thickness of other layers in the sample having various resistivities. Although the method does not permit the absolute determination of the resistivity profile (measurement data would be identical for arbitrary ordered layers having fixed parameters: resistivity and thickness) but it definitely allows to assess resistivity variations in the direction perpendicular to the wafer. The advantage of the method is its extended resistivity measurement range with respect to the commercially available time domain techniques (extending the lower resistivity range). The proposed method covers resistivity range from $5\text{x}10^3$ Ωcm to $10^{10}$ Ωcm.

Materials that are studied in this paper are high resistivity p-type silicon (wafers obtained from TOPSIL, Denmark), undoped gallium phosphide and gallium arsenide (grown by

Manuscript received February 24, 2014; revised July 8, 2014; accepted August 19, 2014. Date of publication September 5, 2014; date of current version November 10, 2014.

J. Krupka is with the Institute of Microelectronics and Optoelectronics, Faculty of Electronics and Information Technology, Warsaw University of Technology, Warszawa 00-665, Poland (e-mail: j.krupka@imio.pw.edu.pl).

J. Judek is with the Faculty of Physics, Warsaw University of Technology, Warszawa 00-662, Poland.

Color versions of one or more of the figures in this paper are available online at http://ieeexplore.ieee.org.

Digital Object Identifier 10.1109/TSM.2014.2352301

0894-6507 © 2014 IEEE. Personal use is permitted, but republication/redistribution requires IEEE permission.
See http://www.ieee.org/publications_standards/publications/rights/index.html for more information.

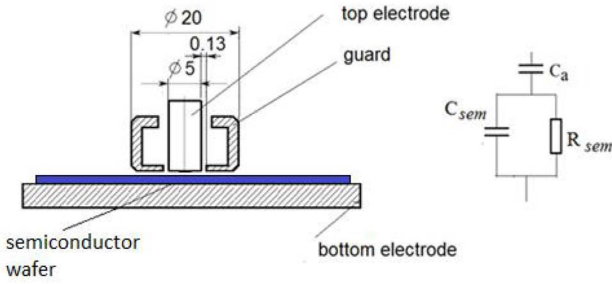


Fig. 1. Agilent Technologies 16451B Dielectric test fixture with guarded electrode having diameter of 5 mm that was used in our experiments.

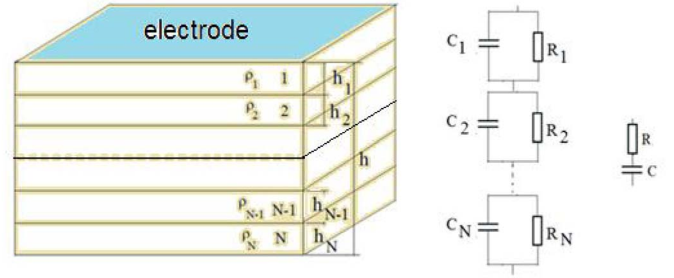


Fig. 2. Multilayer model of semiconductor sample with nonuniform resistivity distribution.

Czochralski method—obtained from the Institute of Electronic Materials Technology, Poland) and high resistivity gallium nitride (grown by ammonothermal process—obtained from AMMONO, Poland). Samples that were studied in this paper were specifically chosen in such a way that they exhibit significant resistivity variations in order to confirm validity of the measurement procedure that is presented in this paper.

## II. Theory

In capacitive measurements sample under test is inserted between two electrodes of air capacitor and together with an air gap above the sample creates a double-layer capacitor. Schematic of capacitive measurement cell used in our experiments is show in Fig. 1.

In the common, simplest approach it is assumed that the equivalent circuit of the measurement cell consists of only three lumped elements: capacitance of air gap above the sample $C_{\mathrm{a}}$, capacitance of semiconductor $C_{\mathrm{sem}}$ and resistance of semiconductor $C_{\mathrm{sem}}$. Let C denote the "effective" capacitance, R denote its "effective" resistance, X denote its "effective" reactance and Q denote its Q-factor, which is defined as $Q = X/R = 1/(\omega RC)$. For such model the Q-factor approaches minima at certain frequencies (maximum loss frequencies) that depend on the resistivity of the semiconductor sample and the capacitances $C_{\mathrm{sem}}$ and $C_{\mathrm{a}}$ according to equation (1) [2].

$$f_{\min} = 1/\left(2\pi R_{\mathrm{sem}}\sqrt{C_{\mathrm{sem}}\left(C_{\mathrm{sem}} + C_{\mathrm{a}}\right)}\right) \quad (1)$$

If the geometry of the capacitive cell, and the permittivity and thickness of the sample under test are known, it is possible to uniquely determine the resistivity of the sample from measurements of the capacitance and the Q-factor at the frequency of the minimum Q-factor $f_{\min}$ (1). In the extended approach that was proposed in [7], semiconductor wafer is considered as a stack of layers having different resistivity values which is schematically shown in Fig. 2.

Complex valued admittance of the n-th single layer is given by the formulae

$$Y_n = G_n + jC_n \quad (2)$$

where:

$$G_n = \frac{S}{\rho_n h_n}, C_n = \frac{\varepsilon_0 \varepsilon_{rn} S}{h_n}$$

S – area of guarded electrode

$\rho_n$, $\varepsilon_{rn}$ and $h_n$ are resistivity, relative permittivity and thickness of the n-th single layer

Resulting equivalent complex impedance $Z$ of the whole multilayer can be expressed as follows.

$$Z = \frac{1}{Y} = \sum_{n=1}^{N} \frac{1}{Y_n} \quad (3)$$

Parameters that are measured with an impedance analyzer are the effective capacitance $C$ and the quality factor Q. They are related to the complex impedance by the following formulas $Q = -Im(Z)/Re\,(Z)$ and $C = -1/\omega Im(Z)$. It should be underlined that measurements of the effective capacitance $C$ and Q-factor in our approach are performed in dozens of points over a broad frequency range. Multi-frequency point measurements data are then used to determine resistivity and thickness of several layers as well as the height of the effective air-gap $h_{\mathrm{a}}$. Geometrical dimensions of the measurement cell, permittivity of the test sample and its thickness are considered as known quantities.

For semiconductor wafers having uniform fixed resistivity in the direction perpendicular to their surface frequency spectra of the effective capacitance and Q-factor look like ideal Debye curves. In such case three parameter model: $\rho$, $h$ and $h_{\mathrm{a}}$ is sufficient to obtain perfect fit to the experimental data over very broad frequency spectrum. If resistivity is non-uniformly distributed the effective capacitance and Q-factor exhibit more complicated behaviour. Let us consider artificial silicon samples having permittivity equal to 11.65 and resistivity distributions as these that are shown in Fig. 3(a) that are inserted into the fixture from Fig. 1. Results of the effective capacitance and Q-factor computations of the fixture with these samples assuming $h_{\mathrm{a}}$=10 $\mu$m are presented in Fig. 3(a) and (b). It should be noted that that for the low frequency limit the capacitance is equal to the capacitance of the air gap $C_0$, while for the high frequency limit the capacitance $C_{\mathrm{inf}}$ is equal to the equivalent capacitance of two capacitors connected in series: the air gap capacitor $C_0$ and the semiconductor sample capacitor $C_{\mathrm{S}}$.

The following conclusions can be drawn from the results that presented in Fig. 3.

1) The effective capacitance and Q-factor at low frequency range is predominantly related to the high resistivity layers, while the high frequency range to the low resistivity layers.
2) Number of layers that are considered in the model have small influence on the effective capacitance and

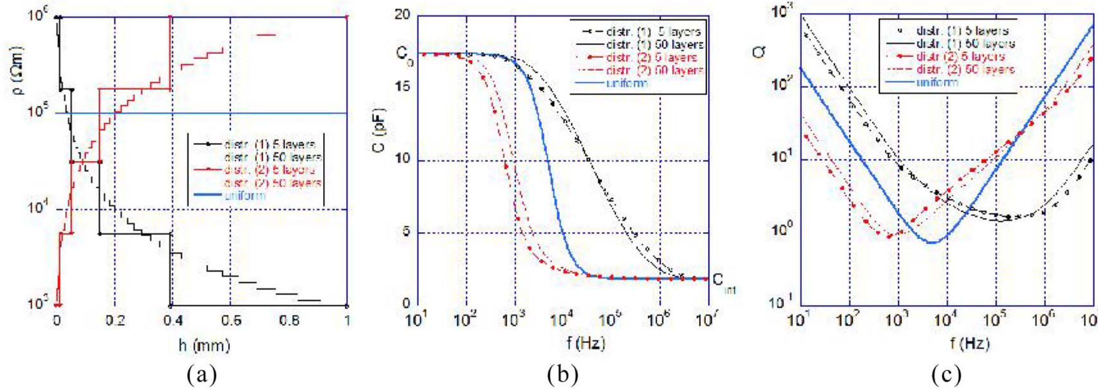


Fig. 3. (a) Resistivity distributions that were assumed in the theoretical analysis. (b) Effective capacitances. (c) Q-factors for artificial silicon samples having permittivity equal to 11.65, thickness equal to 1.0 mm, and the air gap value $h_a$= 10 μm. Capacitances were determined for diameter of the sample equal to 5.0 mm (as for the fixture which is shown in Fig. 1).

Q-factor spectra. It is seen in Fig. 3(b) and (c), where we considered models consisting 5 layers and 50 layers.

3) Positions of the Q-factor minima on the frequency scale are related to the range of resistivities in the subsequent layers. One should note that for the resistivity range from $10^3$ Ωm to $10^6$ Ωm [Fig. 3(a)] the Q-factor minima are situated at the frequencies from $10^3$ Hz (which corresponds to the resistivity of $10^6$ Ωm) to $\sim 10^5$ Hz (which corresponds to the resistivity of $10^3$ Ωm).
4) For measurements that are performed at frequency range from 40 Hz to 15 MHz expected resistivity measurement range is roughly from 5x$10^1$ Ωm to $10^8$ Ωm. This is because only resistivities from such range have measurable influence on the capacitance and Q-factor values in the measured frequency spectrum.
5) For samples with uniform resistivity distribution Q-factor curves are symmetric on the log scale with respect to the frequency of minimum Q-factor while for samples with non-uniform resistivity distribution Q-factor slopes versus frequency are different on both sides with respect to the frequency of the minimum Q-factor.
6) Q-factor slopes are usually steeper for frequencies on the left hand side from the frequency of the minimum Q-factor.
7) Capacitance slopes for samples having uniformly distributed resistivity are steeper that for samples having non-uniformly distributed resistivities.

Real samples of high resistivity semiconductors rarely have uniform resistivity distribution in their volume, so the measurement results of the capacitance and Q-factor over broad frequency range of the sample rarely follow the simple Debye model. Therefore in order to measure resistivity profiles in such samples it is necessary to employ multi-parameter model to determine resistivity and thickness of the subsequent layers of the samples.

## III. Experiments

Measurement of several high resistivity samples have been performed at frequency ranges from 40 Hz to 15 MHz employing Agilent Technologies 16451B Dielectric Test Fixture. For most samples measurements have been undertaken with different air gap settings between the top electrode and the sample. Measurement results of capacitances and Q-factors have been collected and saved on 200 points uniformly distributed in the logarithmic frequency scale. Then the data were used in MATLAB program that employs optimization procedure *fminsearch* to find the vector **p** containing the unknown parameters $\mathbf{p} = [h_a, h_1, \ldots, h_{N-1}, \rho_1, \ldots, \rho_N]$. One should note that the thickness of the last layer is constrained by the requirement: $h_N = h - \sum_{n=1}^{N-1} h_n$, where $h$ is known thickness of the sample. Procedure *fminsearch* (available in the Toolbox OPTIM in MATLAB) finds the minimum of an unconstrained multivariable objective function employing derivative-free Nelder-Mead direct search method [8]. The objective function in our computations had the following form:

$$J(\mathbf{p}, f_m) = \|(C_m(f_m) - C(f_m, \mathbf{p}))/C_m(f_m)\|_2 + \|(Q_m(f_m) - Q(f_m, \mathbf{p}))/Q_m(f_m)\|_2 \quad (4)$$

where: $C_m(f_m), Q_m(f_m), f_m$ typically with $m$=1,..., 200 - the measurement data
$C(f_m, \mathbf{p}), Q(f_m, \mathbf{p})$ - capacitance and Q-factor values obtained from the theoretical model (they are defined below equation (3))
$\|x\|_2$ - the Euclidean norm of $x$

Physically the objective function (4) means the sum of squares of the relative errors between experimental data and theoretical model. In practice the number of parameters to be determined by the optimization procedure, that minimizes the objective function, must be limited. If measurements are performed at frequency range from 40 Hz to 15 MHz (measurement range for Agilent Technologies 16451B Dielectric Test Fixture), few parameter model is sufficient to get good agreement between measurements results and theory. Subsequent measurement results are shown separately for different materials. It should be mentioned that the air gaps between samples and the top electrode were set by the micrometer screw but they were not physically measured. Their heights were obtained from the measurement data in the optimization process.

### A. High Resistivity Silicon

For high resistivity silicon depletion/accumulation and is some cases inversion effects make it difficult to obtain accurate

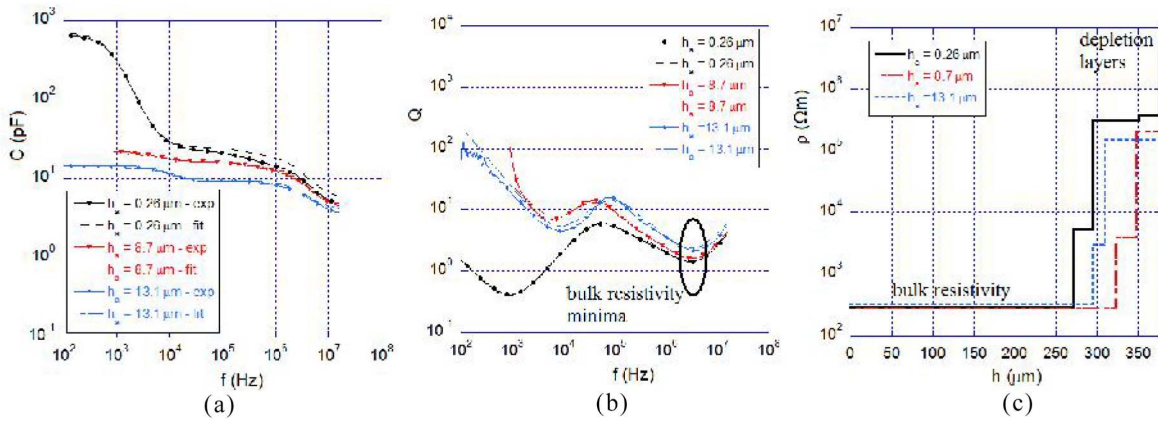


Fig. 4. (a) Capacitance and (b) Q-factor measurements for virgin HR p-type silicon sample having thickness of 376 μm. (c) Resistivity profiles that were obtained employing optimization procedure.

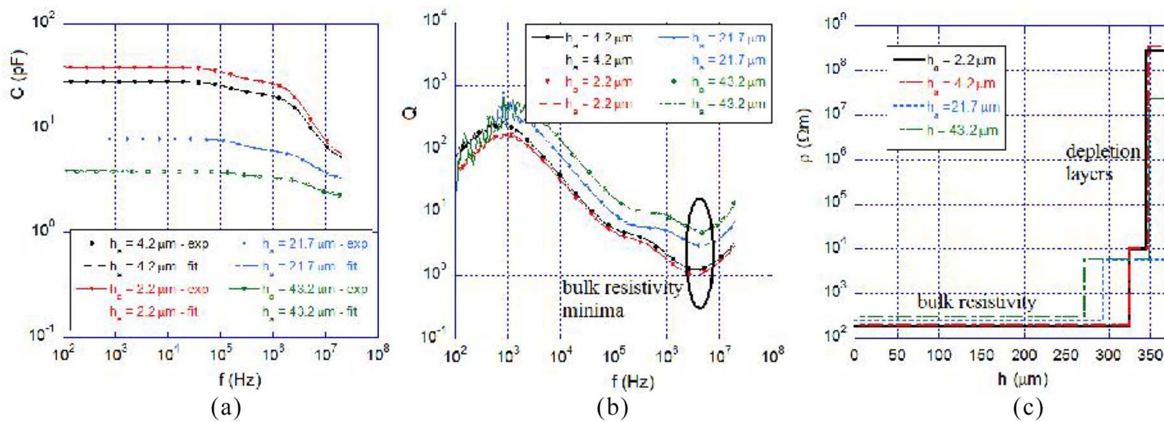


Fig. 5. (a) Capacitance and (b) Q-factor measurements for oxidized HR p-type silicon sample having thickness of 370 μm. (c) Resistivity profiles that were obtained employing optimization procedure.

and reproducible results on the measured resistivity. It is well known phenomenon that the distribution of free charge carriers near surfaces of a silicon wafer significantly varies depending on its surface treatment and its possible oxidation. Also the presence of conducting electrodes on the silicon surface may cause the Fermi level bending on the surface which results in the change of the charge carrier concentration. The higher resistivity of the sample the larger changes of the free carriers concentration near surfaces would be expected. Results of measurements of capacitances and Q-factors of Agilent Technologies 16451B Dielectric Test Fixture containing virgin HR p-type silicon sample having thickness of 376 μm are presented in Fig. 4. Measurements have been performed for three different air gap settings. The effective air gap values that are shown in the labels of all pictures in Fig. 4 were obtained employing optimization procedure. It should be noted that the resistivity of the dominant part of the sample having thickness in the range of 275-325 μm is almost constant. Its average value is equal to 298 Ωm which is very similar to the values measured on the same sample employing four point probe method $\rho_{DC}$ = 280 Ωm (+/-) 20 % and using the microwave split post dielectric resonator method [4] $\rho_{micro}$ = 278 Ωm (+/-) 5 %. Although resistivity of the bulk part of the sample is almost constant but thickness and resistivity of depletion layers vary depending on the air gap setting.

This means that vicinity of a metal electrode results in the Fermi level bending and changing the depth of depletion layers. Additional experiments on the same sample have also shown dependence of the properties of depletion layers (thickness and resistivity) on the cleaning process of the sample.

The next experiment have been performed on the HR p-type silicon sample from the same batch as the first virgin sample but oxidized - with oxide layers having thickness of 300 nm grown on both sides of the sample. Resistivity values measured on this sample before oxidation were: with the four point probe method $\rho_{DC}$ = 230 Ωm (+/-) 20 % and with the microwave split post dielectric resonator method $\rho_{micro}$ = 225 Ωm (+/-) 5 %. After oxidation sample was not measurable by four point probe method due to the presence of relatively thick silicon oxide layers on both sides of the wafer, but its resistivity measured by the microwave split post dielectric resonator method dropped to the value $\rho_{micro_ox}$ = 8 Ωm (+/-) 5 %. Results of measurements of capacitances and Q-factors of Agilent Technologies 16451B Dielectric Test Fixture containing the oxidized silicon sample are presented in Fig. 5(a) and (b), and its resistivity profile in Fig. 5(c).

It is seen that the resistivity of the dominant part of the sample having thickness in the range of 275-325 μm is almost constant being equal to 227 Ωm (+/-) 20 %. Very large

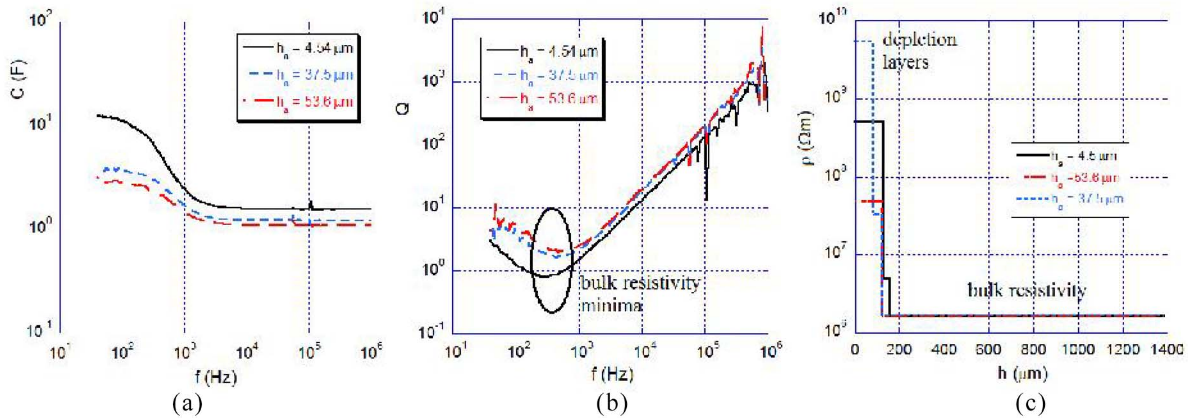


Fig. 6. (a) Capacitance and (b) Q-factor measurements for GaAs sample having thickness of 1380 μm. (c) Resistivity profiles that were obtained employing optimization procedure.

difference (28 times) between the split-post dielectric resonator and the capacitive frequency domain methods can be explained as the results of the appearance of inversion layers below the layers of silicon oxide. The origin of the inversion layers is the presence of high concentration of positive charges in the silicon oxide. In the split post dielectric resonator the electric field and electric currents are circumferential in the plane of the sample so the layers with the minimum sheet resistance (the inversion layers) have the dominant influence on the measured (average) resistivity value. Contrary in the RF capacitive method the electric field and the electric currents are perpendicular to the sample surfaces so the influence of the inversion layers on the capacitance and Q-factor curves is not seen. After etching off the silicon oxide layers the effective resistivity, measured with the microwave method, have increased but only by a factor of 10 to compare to the oxidized silicon sample. This means that after etching process shallow inversion layers still exist due to the presence of in-built charges on the silicon surfaces or due to unintentional doping of the sample during the high temperature thermal oxidation process.

### B. Gallium Arsenide

Semi-insulating, nominally undoped gallium arsenide sample having thickness of 1380 μm was cut from the ingot grown by Czochralski method at the Institute of Electronic Materials Technology. Its nominal resistivity was specified to be larger than $10^7$ Ωcm. Capacitance and Q-factor measurements for this sample are shown in Fig. 6(a) and (b) respectively. Measurements have been performed for three different air gap settings. For each measurement sets three layer model of semiconductor sample was used to obtain resistivity and thickness of particular layers as well as the air gap heights. Results of computations are shown in Fig. 6(c). It is seen that resistivity of the bulk part of the sample, being equal to $1.63 \times 10^6$ Ωm, does not depend on the air gap settings but resistivity and thickness of the depletion layers depend on them, similarly as for silicon samples. Measurements performed at different areas of the sample were very similar to those that are presented in Fig. 6 so the bulk resistivity of the sample can be considered as a constant value.

The presence of depletion layers in GaAs sample is clearly seen in Fig. 6(a) especially for the gap setting equal to 4.54 μm because the slope of capacitance versus frequency at the lowest measured frequency is not equal to zero as it would be expected for a sample having uniform resistivity.

### C. Gallium Phosphide

Two gallium phosphide samples having thickness of 765 μm and 460 μm were cut from two different ingots grown by Czochralski method at the Institute of Electronic Materials Technology. They are nominally undoped and they should have resistivity larger than $10^6$ Ωcm. Capacitance and Q-factor measurements for the first sample are shown in Fig. 7(a) and (b) respectively. Measurements have been performed for four different air gap settings. For each measurement sets three layer model of semiconductor sample was used to obtain resistivity and thickness of particular layers as well as the air gap heights. Results of computations are shown in Fig. 7(c). It is seen that resistivity of the bulk part of the sample, is almost constants $6.5 \times 10^3$ Ωm (+/-) 5%, but resistivity and thickness of another layers depend on the air gap settings.

For the air gap setting equal to 9.7 μm, the branch of the Q-factor curve that is on the left from minimum (at low frequency range) has much less steep slope than for another curves, which means the presence of additional higher resistivity layers (depletion layers). For large air gap settings lower resistivity regions are present. We should admit however that the accuracy of resistivity determination for the low resistivity regions is rather poor because it is derived from the part of measurements at the highest frequencies.

The second gallium phosphide sample having diameter of 50.4 mm and thickness of 460 μm was defected and four point probe measurements on the sample were not reliable showing values from about 1000 Ωcm to infinity (contact error). Measurements on this sample have been performed employing two methods: the microwave split-post dielectric resonator method [4] and the capacitive frequency domain method. The first method was used to obtain resistivity profiles in the plane of the sample probed with circumferential currents as it is seen in Fig. 8(a), and the second was used to obtain vertical

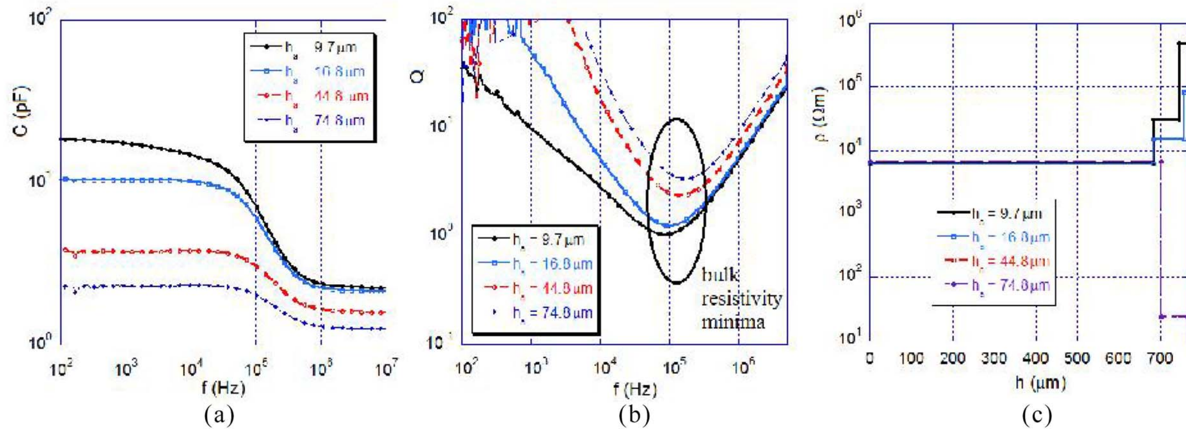


Fig. 7. (a) Capacitance and (b) Q-factor measurements for GaP having thickness of 765 µm. (c) Resistivity profiles that were obtained employing optimization procedure.

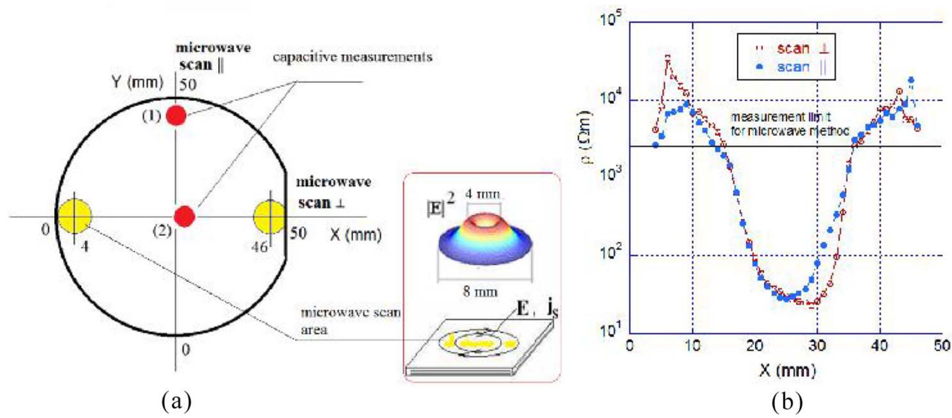


Fig. 8. (a) Schematic picture of microwave mapping. (b) X-Y plane resistivity profile for GaP sample having diameter of 50.4 mm and thickness of 460 µm measured with split post dielectric resonator scanner (at 14.6 GHz).

resistivity profiles at two different points of the sample that are marked with red circles in Fig. 8(a). Results of microwave measurements are shown in Fig. 8(b). It is seen that resistivity profile exhibits distinct minimum near the center of the sample. The average in the plane microwave resistivity of the sample at this point is equal to ñ$_{mic_av} = 22.9$ Ωm.

It should be noted that the average resistivity $\rho_{av}$ measured in the plane of the sample with the split post dielectric resonator method is related to restivities $\rho_n$ and thickness's $h_n$ of $N$ layers by the following formulae.

$$\rho_{av} = h / \sum_{n=1}^{N} h_n / \rho_n \tag{5}$$

This is because for circumferential currents the sheet resistances of individual layers are connected in parallel. Capacitance and Q-factor measurements at two different points of this gallium phosphide sample are shown in Fig. 9(a) and (b) respectively and vertical resistivity profiles which were determined at these points are presented in Fig. 9(c).

Resistivity profile at the point (1) shows semi-insulating character with resistivity variations from 2x$10^4$ Ωm to $10^8$ Ωm. Resistivity profile at the point (2) exhibits much larger resistivity variations from about 4 Ωm to $10^7$ Ωm. Again it should be mentioned that the accuracy of resistivity determination for the lowest resistivity region is rather poor because it is related to the part of measurements at the highest frequencies. Using the data from Fig. 9(c) we have evaluated the average in the plane resisistivity of the sample at the point (2) employing formulae (5). The result which was evaluated for the air gap setting equal to 7.8 µm was the closest to measured microwave value and was equal to ñ$_{RF_av} = 17.4$ Ωm. Because the microwave resistivity depends predominantly on the resistivity of the most conductive layer one can conclude that the resistivity of this layer determined with the capacitive technique is underestimated, especially for the largest air gap setting, but still the agreement between the microwave and the capacitive method is good for such extremely non-uniform sample.

### D. Gallium Nitride

To grow single crystals of gallium nitride AMMONO company implemented the ammonothermal technique [9]. The typical temperatures and pressures applied in this technique are 0.1 - 0.3 GPa and 500 °C - 700 °C, respectively. In addition, the use of mineralizers (LiNH2, NaNH2 or KNH2) is

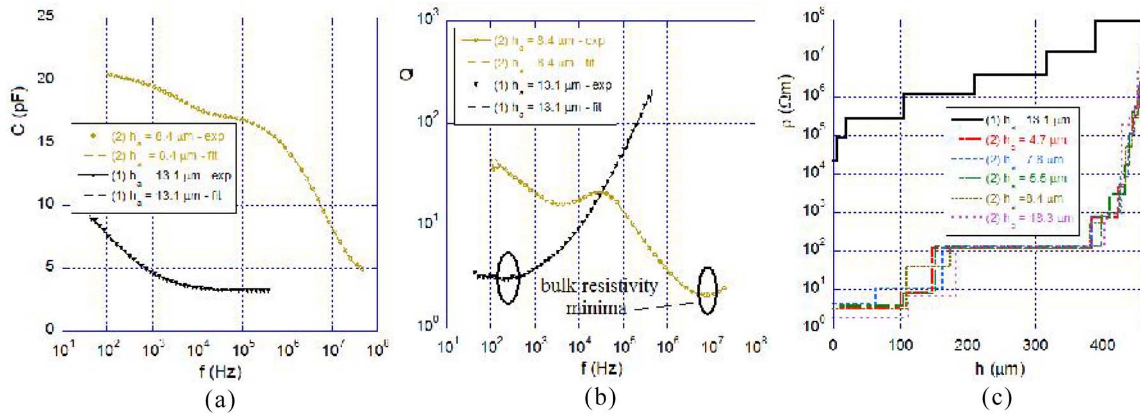


Fig. 9. (a) Capacitance and (b) Q-factor measurements for GaP sample having thickness of 460 μm measured at two points marked with (1) and (2) in Fig. 8(a). (c) Resistivity profiles determined from capacitive measurements, at points (1) and (2), with different air gap settings.

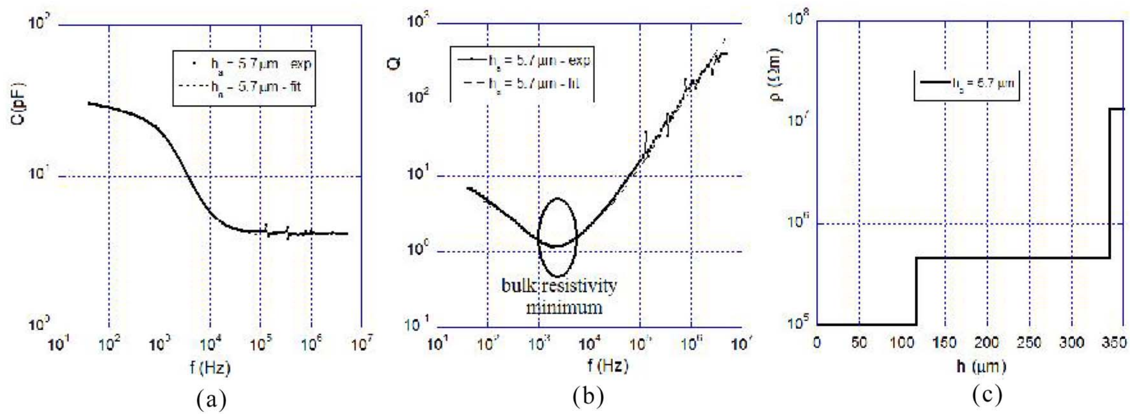


Fig. 10. (a) Capacitance and (b) Q-factor measurements for GaN sample having thickness of 360 μm. (c) Resistivity profiles that were obtained employing optimization procedure.

necessary in order to enhance the solubility of GaN in ammonia. The electrical properties of GaN wafers that have diameters up to 2” and thickness of few hundred μm are controlled by appropriate doping. One important class of products manufactured by AMMONO are semi-insulating GaN substrates. To measure their resistivity both capacitive frequency domain and split post dielectric resonator techniques are used. Typically most of semi-insulating GaN substrates (as grown) exhibit resistivity in the range $10^5$ Ωm to $10^9$ Ωm which is measured by frequency domain capacitive technique. Wafers may exhibit various resistivity profiles in the direction perpendicular to them. Measurement results for 1.5” GaN wafer having thickness of 360 μm are presented in Fig. 10. High temperature annealing (1300 °C for 1 hour) of some semi-insulating GaN wafers may cause appearance of a low resitivity layer on a one side of the substrate (probably caused by the segregation of dopants). Similarly as for the oxidized silicon sample the presence of such low resistivity layers cannot be detected with the capacitive technique but their presence is clearly visible in the microwave measurements.

For non annealed semi-insulating wafers their microwave resistivity is always > $2\text{x}10^5$ Ωcm (measurement limit for microwave methods) while for annealed wafers it may drop down even below 1000 Ωcm. The internal part of such wafer remains semi-insulating which can be measured with the capacitive technique. After polishing off the layer of 2-3 μm thick from the conducting surface of the wafer, its microwave resistivity becomes again larger than $2\text{x}10^5$ Ωcm. Thus simultaneous use of the frequency domain capacitive technique and the microwave split post dielectric resonator technique enables to measure resistivity profiles in broad range of resistivities as well as to detect and measure the sheet resistance of low resistivity layers.

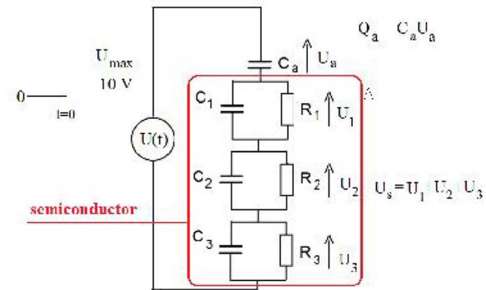


Fig. 11. Equivalent capacitive cell model that have been used in time domain analysis.

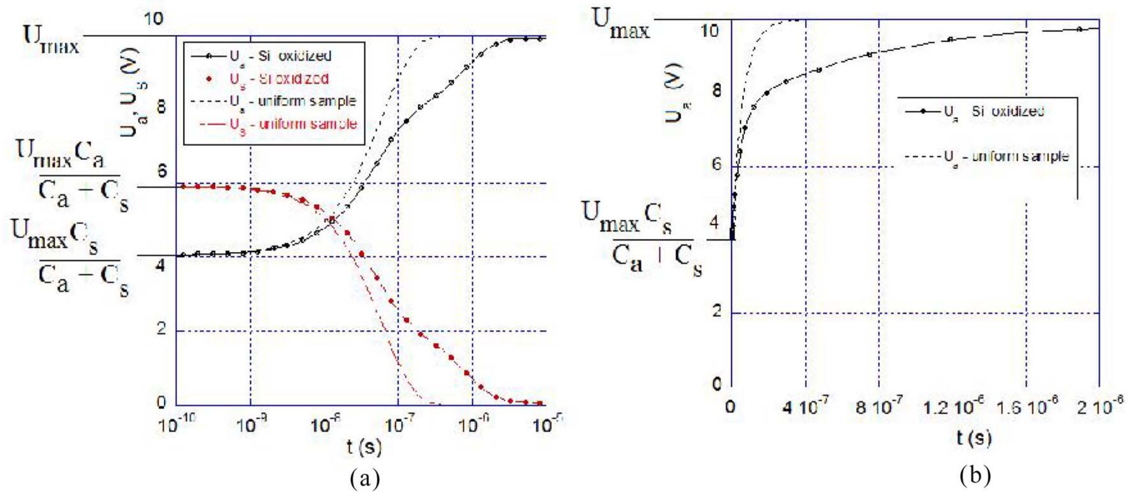

Fig. 12. Time domain responses, in logarithmic (a) and in linear (b) time scales, of the equivalent circuit that is shown in Fig. 11 for oxidized silicon sample with $h_a$ = 21.7 μm, $h_1$ = 294 μm, $\rho_1$= 240 Ωm, $h_2$ = 74.2 μm, $\rho_2$= 5.62 × $10^3$ Ωm, $h_3$ = 1.8 μm, $\rho_3$= 6.0 × $10^6$ Ωm, and a silicon sample having constant resistivity and $h_a$= 21.7 μm, $h$ = 370 μm, $\rho$ = 240 Ωm. $U_a$-voltage on the air capacitance, $U_S$-total voltage across semiconductor sample (sum of voltages $U_1$, $U_2$, and $U_3$).

## IV. Influence of Nonuniform Resistivity Distribution on the Capacitive Time Domain Measurements-Theoretical Analysis

In commercially available time domain capacitive measurement systems three element model of the capacitive cell (air gap and a single layer semiconductor having uniform resistivity) is usually employed. In this section we will analyse the influence of non-uniform resistivity distribution on the voltage-time responses for a more complicated model of semiconductor loaded capacitive cell. This model is schematically shown in Fig. 11.

The voltage-time responses of the equivalent circuit, which is shown in Fig. 11, have been analyzed by solving the system of four ordinary differential equations with respect to the four voltages $U_1$, $U_2$, $U_3$ and $U_a$ with the stiff differential equation solver *ode23s* in the MATLAB environment. The algorithm which is implemented in the *ode23s* solver uses modified Rosenbrock formula of order 2. It has been assumed that at the time instant t = 0, a pulse step voltage with a magnitude of 10 V is applied to the circuit from Fig. 11. Results of computation of the time-dependent voltages on the capacitors $C_a$ (air) and $C_s$ (semiconductor) are shown in Fig. 12(a) in the logarithmic time scale and in Fig. 12(b) in the linear time scale. It should be noted that in descriptions of capacitive resistivity evaluation employing time domain technique usually charge transient curves instead of voltage transient curves are presented [1]. Both charge and voltage approaches are equivalent because by definition the charge $Q_a$ on the capacitance $C_a$ is equal to the product of the voltage $U_a$ and the capacitance $C_a$ i.e. $Q_a = U_a\ C_a$ and, for a fixed air gap value the air capacitance, $C_a$ is constant.

Two different silicon samples have been considered in our computation. The first one was real oxidized silicon sample that was analyzed in Fig. 5 with air gap setting $h_a$= 21.7 μm and $h_1$ = 294 μm, $\rho_1$=240 Ωm, $h_2$ = 74.2 μm, $\rho_2$=5.52x$10^3$ Ωm, $h_3$ = 1.8 μm, $\rho_3$=6.0x$10^6$. The second was hypothetic silicon sample having constant resistivity $\rho$=240 Ωm and h = 370 μm with air gap setting $h_a$= 21.7 μm. It is seen that voltage-time responses for the two samples are substantially different due to the presence of depletion layers in the oxidized sample. Thus the bulk resistivity of the oxidized silicon sample would not be determined accurately from the ordinary time-domain measurements, that are based on the simple model of semiconductor.

The same would be true for other samples having non-uniform resistivity distribution. In principle modification of the time-domain measurements is possible employing multi-layered model of semiconductor (multi relaxation time model) and voltage-time measurements over a large number of points. Then, similarly as for the frequency domain technique, optimization procedure can be used to obtain the vector of parameters of the model that provides the best fit to the experimental data. This is a task that should be undertaken by manufacturers of capacitive time-domain resistivity measurement systems.

## V. Conclusion

Employing multilayer model of semiconductor wafer we have shown that vertical resistivity variations inside the wafer significantly affect the frequency dependencies of the measured effective capacitance and the Q-factor. From the experimental data: C(ω) and Q(ω) measured on Si, GaAs, GaP and GaN samples we have determined their profiles (thickness and resistivity of few layers) employing optimization procedure. It has been shown that high resistivity samples exhibit non-uniform resistivity distribution in the direction perpendicular to the wafer due to the presence of depletion, accumulation and inversion layers. Theoretical analysis of the influence of non-uniform resistivity distribution on capacitive time domain measurements has been performed showing necessity for using multilayered model of semiconductor wafer when measurements on the samples with non-uniform resistivity are conducted.

It should be mentioned that combination of the two techniques (RF and microwave) allows to detect various resistivity imperfections such as the presence of inversion and depletion layers in expensive GaN substrates to improve their quality. Both the capacitive frequency domain method, which is described in this paper, and the split post dielectric resonator technique have been already used for quality control of semi-insulating GaN wafers manufactured by AMMONO company.

## REFERENCES


[1] R. Stibal, J. Windscheif, and W. Jantz, "Contactless evaluation of semi-insulating GaAs wafer resistivity using the time-dependent charge measurement," *Semicond. Sci. Technol*. vol. 6, no. 10, pp. 955–1001, 1991.

[2] D. Siebert and F. Matossi, "Untersuchungen zum Photokapazitiven Effekt von Phosphoren," *Phys. Kond. Mater.,* vol. 2, no. 4, pp. 334–354, 1964.

[3] W. R. Thurber, J. R. Lowney, R. D. Larrabee, and J. R. Ehrstein, "AC impedance method for high−resistivity measurements of silicon," *J. Electrochem. Soc*., vol. 138, no. 10, pp. 3081–3085, 1991.

[4] J. Krupka, "Contactless methods of conductivity and sheet resistance measurement for semiconductors, conductors and superconductors," *Meas. Sci. Technol.,* vol. 24, no. 6, 2013, Art. ID. 062001.

[5] J. R. MacDonald, *Impedence Spectroscopy-Emphasizing Solid Materials and Systems*. New York, NY, USA: Wiley, 1987.

[6] *SemiMap Scientific Instruments GmbH* [Online]. Available: http://www.semimap.de

[7] J. Krupka, "Contactless methods of both conductivity and sheet resistance measurements of semiconductor crystals, wafers and epitaxial films deposited on semi-insulating substrates," in *Proc. 17th Int. Conf. Cryst. Growth Epitaxy*, Warsaw, Poland, Aug. 2013.

[8] J. C. Lagarias, J. A. Reeds, M. H. Wright, and P. E. Wright, "Convergence properties of the Nelder–Mead simplex method in low dimensions," *SIAM J. Optim.*, vol. 9, no. 1, pp. 112–147, 1998.

[9] R. Dwiliński *et al.*, "Bulk ammonothermal GaN," *J. Cryst. Growth,* vol. 311, pp. 3015–3018, 2009.


**Jerzy Krupka**, photograph and biography not available at the time of publication.

**Jaroslaw Judek**, photograph and biography not available at the time of publication.